SCIENTIFIC REPORTS

OPEN

SUBJECT AREAS:
SINGLE-MOLECULE BIOPHYSICS
NANOSCALE BIOPHYSICS

Received
9 October 2013

Accepted
19 December 2013

Published
27 January 2014

Correspondence and requests for materials should be addressed to I.A. (andricio@uci.edu) or T.L. (luchian@uaic.ro)

* These authors contributed equally to this work.

# Slowing down single-molecule trafficking through a protein nanopore reveals intermediates for peptide translocation

Loredana Mereuta[1]*, Mahua Roy[2]*, Alina Asandei[3], Jong Kook Lee[4], Yoonkyung Park[4], Ioan Andricioaei[2] & Tudor Luchian[1]

[1]Department of Physics, Alexandru I. Cuza University, Iasi, Romania, [2]Department of Chemistry, University of California, Irvine CA 92697, USA, [3]Department of Interdisciplinary Research, Alexandru I. Cuza University, Iasi, Romania, [4]Research Center for Proteineous Materials, Chosun University, Gwangju, South Korea.

**The microscopic details of how peptides translocate one at a time through nanopores are crucial determinants for transport through membrane pores and important in developing nano-technologies. To date, the translocation process has been too fast relative to the resolution of the single molecule techniques that sought to detect its milestones. Using pH-tuned single-molecule electrophysiology and molecular dynamics simulations, we demonstrate how peptide passage through the α-hemolysin protein can be sufficiently slowed down to observe intermediate single-peptide sub-states associated to distinct structural milestones along the pore, and how to control residence time, direction and the sequence of spatio-temporal state-to-state dynamics of a single peptide. Molecular dynamics simulations of peptide translocation reveal the time- dependent ordering of intermediate structures of the translocating peptide inside the pore at atomic resolution. Calculations of the expected current ratios of the different pore-blocking microstates and their time sequencing are in accord with the recorded current traces.**

A host of crucial biological processes rely on peptide trafficking through nanopores inserted into membranes that delimit various cellular compartments. Examples include protein import inside mitochondria[1] or the endoplasmic reticulum[2], protein transport across the chloroplast membrane[3] or the nuclear envelope of eukaryotic cells[4], protein sorting to the peroxizomes[5] and proteins translocated upon viral DNA ejection in bacteriophages[6]. Due to the delicate interplay of many key molecular interactions, the biology of the process in itself is rich in details, as is the range of nanotechnology applications involving peptide sequencing and sorting through natural[7] and artificial nanopores[8–10]. The underlying technique for nanopore transport studies is the Coulter counter, resistive-pulse technique[11], in which an external electric field ushers the passing macromolecules one at a time into the nanopore, leading to transient blockades of the electrical current through the pore. The amplitude, duration and rate of the blockades can reveal the identity and concentration of the macromolecule, and the interactions between the macromolecule and the nanopore can be studied in real-time at high resolution.

Versatile with respect to their size, shape, and function, either solid-state or protein-based nanopores are excellently suited for studying at the single-molecule level peptides- and proteins-pores interactions in-vitro[7–10,12–14], in order to gain valuable knowledge regarding the microscopic description of the biological processes mentioned above. The large majority of the studies focusing on the molecular details of protein and peptide unfolding or translocation through nanopores employed solid-state nanopores as model translocation systems[15–17] graphene nanopores[18] and a variety of protein channels including α - hemolysin (α - HL)[19–25], OmpF[26,27], aerolysin[28,29], the MspA channel[30] or the Phi29 connector channel[31]. The potential of resistive-pulse technique, in effect tracing structural dynamics from the time series recordings of the single-pore current, was originally revealed by sensing single polymers in buffers[32], and was soon followed by the proof of the principle demonstration of the possibility to detect RNA and DNA molecules[33], and to separate molecules at high resolution[34–36]. In addition, protein unfolding transitions were investigated in the presence of denaturing agents[16], or in the presence of extrinsic factors such as temperature[37] or electric fields[38]. Through extensive computational studies as multiscale modeling and atomistic simulations, experimental results have been excellently complemented, both for solid and biological nanopore[23,39–46].

The α-HL protein secreted by *Staphylocous aureus* is arguably the nanopore of choice for single-molecule protein translocation studies via electrical recordings in artificial lipid membranes. α-HL is structurally stable, electrically-silent over a wide range of experimental conditions[47], its crystal structure has been resolved[48], and can be genetically engineered with tailored chemical functionality. As such, it is archetypal for a wide range of translocation studies[16,37,38]. Instrumental as they have been in single-molecule technique development, all existing peptide translocation studies have suffered so far from the problem that the time-sequencing of any intermediate events evaded detection. This was because translocation was too fast relative to the time resolution of single molecule current recording. Therefore, any information about the peptide moving along the different structural compartments of the pore and/or undergoing major conformational changes in the nanopore was undetectable. A significant advance was recently reported by Rodriquez-Larea and Bayley[49], who demonstrated that distinct unfolding states can be observed in single channel current recording of thioredoxin passing through α–HL if the protein was pulled inside the pore by the attachment of a long exogenous DNA polymer. Herein, we are interested in observing intermediates upon passage not for DNA-attached peptides, but for free peptides, i.e., for peptides that pass freely the pore, rather than being actively pulled through by one end. Moreover, we are interested in relatively small peptides that can obturate the pore in folded, compact states rather than being unfolded by pulling them through from one of their termini. To this end, we chose a 20 amino acids short peptide with a particular choice of two critical Gly residues which can form a kinked, folded beta-hairpin like structure whose size is just right to "clog" the pore. In the realm of DNA, the reduced ability to slow down translocation and the need to optimally adjust the time resolution of signals reflecting intermediates and to accurately determine the amplitude and duration of blockages were addressed by devising several strategies. The most practical ones ruled out the need to modify the translocating molecule or the nanopore itself and involved altering readily accessible experimental parameters, such as the driving voltage, buffer properties and temperature[50–52].

To slow down peptide translocation so that we can detect intermediates, we took a fundamental look at the two components modulating peptide translocation speed in our case: electrophoresis and electro-osmosis. Seeking ways to alter the relative contribution of the two enabled us to devise a strategy capable of monitoring translocation intermediates. This strategy involved varying the solution pH, which was also successful in controlling DNA translocation time through solid-state[53]. The advantage of our technique for the more complex hemolysin pore, with its topologically distinct chambers (β-barrel vs. vestibule) is that different sub-states on the translocating pathway can be identified, controlled and kinetically quantified for the first time. Moreover, the slow-down occurs for free peptide states in the pore, i.e., in the absence of external pulling attachments. We employed peptide engineering, single-molecule electrophysiology, and molecular simulations to obtain several insights into the microscopic description peptide interaction with the α–HL protein. We focused on analogues of the **c**ecropin **A**–**ma**gainin antimicrobial chimera peptide (termed CAMA), and analyzed the association and translocation of peptides through a membrane-immobilized α - HL protein pore. Various parameters that characterize at the single molecule level the peptide-protein nanopore interactions, such as the frequency of current blockades, the translocation rate, the extent of peptide-induced blockades and magnitude of the residual current, were extracted from current signatures collected at several pH values over a range of potentials. Our data suggest that the barrier to peptide capture can be easily controlled by modulating the flow through the α - HL β-barrel, via changes in the pH alone. For the first time to our knowledge, we show how, as the peptide exits the pore at the single-molecule level, the manipulation of the charged state of the α-HL permeating pathway, via pH changes in the buffer, allows to discriminate between two consecutive pore translocation steps: passage through the β-barrel region and through its vestibule. The analysis of the first-passage time distribution of peptide transport through the α–HL vestibule revealed that the electro-osmotic flow is the pH-dependent factor that modulates peptide translocation, and dominates over the electrophoretic flow at acidic pH values.

## Results

Following the formation of a robust lipid membrane, a successful insertion of a single α-HL protein pore, added from the cis side of the membrane results in an 'open pore' trans-membrane current $I_o$ = 81.6 ± 2.8 pA measured at a potential +50 mV, in a buffered solution containing 2 M KCl at pH = 7. When exposed to the CAMA P6 peptide (KWKLFKKIGIGKFLQSAKKF-NH2) added on the trans side of the membrane (i.e., on the β-barrel side of the pore) at a bulk concentration of 30 μM, a transient decrease in the α-HL open pore current *vs.* time occurs in a stochastic manner, reflected by downwardly pointing spikes (Fig. 1). As reported before[19,20], we attribute these spikes to molecular events whereby a single peptide enters the protein β-barrel and induces reversible partial blocks of the ionic current through steric occlusions of the ion permeation pathway, before getting released to the cis side of the membrane under the influence of the potential imposed across the pore, positive on the peptide side addition. We stress that in all the analyses we excluded the distinct population of very fast occurring, low-amplitude spikes, which reflected blockage events due to peptide bumping into the pore mouth, and not the actual capture events of the peptide into the inner region of the α - HL′s β-barrel that eventually lead to the electrophoretic translocation of the peptide to the cis side of the membrane.

Around neutral pH, the interaction between a peptide and the protein β-barrel leads to homogenous blocking events, whose relative block on the current flow through the open protein ($\Delta I\ B_1 = I_{B1} - I_O$) is associated to the $B_1$ blockage sub-state (Fig. 1, panel a). Zooming-in for details in the recorded current traces (see Fig. 1, panels b, c and d) revealed that, as the buffer pH drops, a second blockage sub-state, denoted $B_2$, of a reduced relative magnitude ($\Delta I\ B_2 = I_{B2} - I_O$) becomes apparent. The α-HL's β-barrel (inner diameter of ~20 Å) and its vestibule (average diameter of ~46 Å) have distinct sizes and distinct chemical and topological properties[8]. This results in distinct current blockades when the peptide resides in one of the two distinct chambers. Invoking volume-exclusion arguments, we attribute the higher blockage level (denoted by $B_1$) to the peptide residing in the β-barrel, and the lower blockage level (denoted by $B_2$) to the peptide inside the vestibule. Thereafter, peptide released to the cis side of the membrane completely unblocks the pore (Fig. 1). Molecular dynamics simulations at neutral pH confirm this sequential journey and show a larger transversal accessible area when the peptide passes through the vestibule than through the β-barrel (Fig. 2, panel f). Similar current assignments were applied to the investigation of polynucleotide translocation across α-HL[54,55]. In further support to this assertion, the close analysis performed on all experimental traces demonstrated the sequential occurrence of these intermediary-blocking events. Namely, when the peptide is added to the trans side, level $B_1$ appeared always before level $B_2$, ruling out the possibility that a peptide, which has threaded through the constriction region to the vestibule, retracts back into the protein β-barrel. Conversely, when the peptide was added on the cis side of the membrane, the interaction between a single CAMA P6 peptide and the membrane-inserted α-HL, in all instances gave rise first to a relatively small blockage sub-state $\Delta I\ B_2$ (cis) = 38.21 +/− 0.55 pA reflecting the peptide interaction with the vestibule, that was followed sequentially by a larger blockage sub-state $\Delta I\ B_1$ (cis) = 72.49 +/− 0.43 pA, associated to the peptide residence within the β-barrel (Fig. S1). Moreover, recordings made at lower pH (to ensure the slow-down

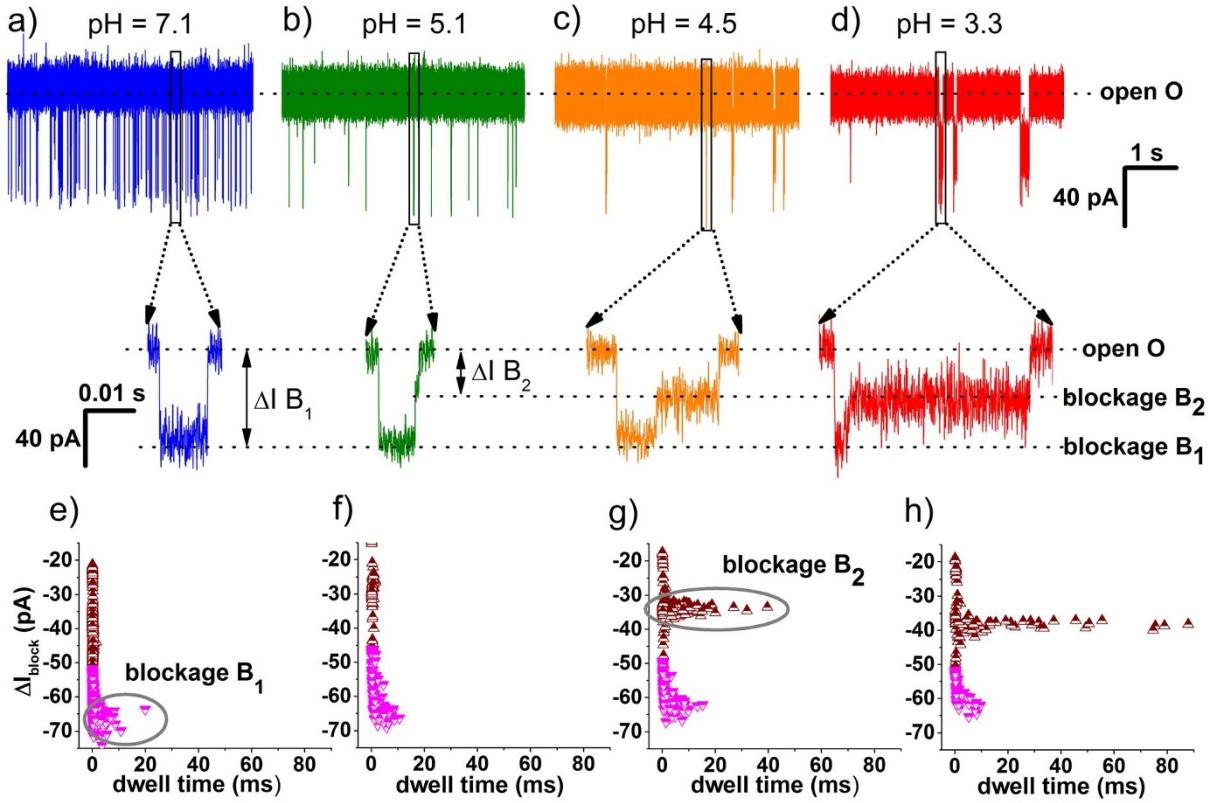


**Figure 1 | Typical single-pore current recordings reflecting peptide interaction with the α-HL pore immobilized in a lipid membrane.** All traces recorded at +50 mV, in symmetrical 2 M KCl at pH = 7.1 (panel a), pH = 5.1 (panel b), pH = 4.5 (panel c) and pH = 3.3 (panel d) with 30 μM peptide applied to the trans side of the membrane. Dotted line in panels a-d shows level of open-pore current before a peptide partitioned within the β-barrel; downward spikes reflect stochastic reduction of pore current induced by the reversible association of a peptide with an open protein pore. The zoomed-in trace segments under each panels a–d reveal the distinct blockage sub-states, $B_1$ and $B_2$ (see text) associated with a single peptide in the pore at various pH values. The distinct sub-states are visualized in panels (e)–(h), scatter plots of dwell time vs. relative blockage amplitude of blockage events. For exemplification, we highlight by encircling the $B_1$ state at neutral pH (panel e), and the $B_2$ state at pH = 4.5 (panel g).

of the peptide movement) revealed oscillations between sub-states $B_1$ to $B_2$ (Fig. S2), directly indicating that the peptide travels back and forth along the two compartments of the protein pore. This sequence of spatio-temporal events associated to peptide transient residence in particular regions of the pore in low pH buffers, when the peptide was added on either side of the membrane, is seen directly for the first time to our knowledge. Even more convincingly, the fact that in certain cases, sub-state O follows sub-state $B_1$ or sub-state $B_2$ (Fig. S2) constitutes direct proof of the direction in which the initially vestibule-trapped peptide gets released, namely to the trans or cis side of the membrane.

Further insight into the microscopic details of the conformational ensemble the peptide can adopt in states $B_1$ and $B_2$ observed in the single-molecule recordings was revealed from the molecular dynamics simulations of the peptide in the α-HL pore with both peptide and protein at atomic details (see Fig. 2 and methods for details). In the simulations, the peptide was subjected to an electrical driving force via the application of a trans-membrane voltage across the protein pore. However, given the intrinsic limitation of simulations, this electrical driving force is an order of magnitude higher than experimental values so as to observe a complete translocation event. Three types of peptide structures were observed in the simulations. The first type is that in the free state, where the peptide takes in a heterogeneous, floppy kinked shape given by the turn-forming propensity of the two alternate glycines (G) at positions 9 and 11 separated by one isoleucine (I) at position 10 (Fig. 2, panel a). Otherwise than the G-formed kinks, the conformations of the other residues are random in solution. In the confines of the β-barrel, the peptide takes on a second "hairpin-like" kinked conformation that clogs the β-barrel (Fig. 2, panel b). Additionally, the kinked fold of the peptide is stabilized by inter-residue hydrogen bonding (this also occurs but to a lesser extent in the free state). We stress however that the kinked hairpin-like state is not a true beta hairpin. A third peptide structure is also observed in which the peptide extends and passes through the constriction as a linear chain (Fig. S3). The peptide inside the β-barrel taking up the intermediate kinked, "folded" structure causes full current blockage (state B1). Upon passage in the vestibule, partial clogging of the pore leads to an intermediate value of the current signals (B2), which we assign to the peptide sampling the vestibule (Fig. 2, panel c). The linear unfolded peptide threaded in the pore observed in the simulations has relevance (as discussed later in the text) to the unfolding effect of low pH conditions.

From the simulation, we calculated for each snapshot along the dynamics of the translocation the transversal (cross-sectional) area $S(z)$ through which the current flows at each depth $z$ along the axis of the pore. The three major states of openness of the pore are observed, assigned to when the peptide resides in the β-barrel, in the vestibule and when the pore is open (Fig. 2, panel f). The ratio of the residual current when the peptide is in the β-barrel/vestibule vs. the open channel current can be modeled by integrating the $z$ dependent resistance (see SI, equation (10) and Fig. S4). This has been used in the simulations to generate the data for residual current (Fig. S5, panel a), in both $B_1$ and $B_2$ states (see Table S1). While the experimental values, being pH dependent (pH ~ 3.3–5.1), range between 0.25–0.15 for $B_1$ state and 0.51–0.73 for $B_2$ state, the calculated values

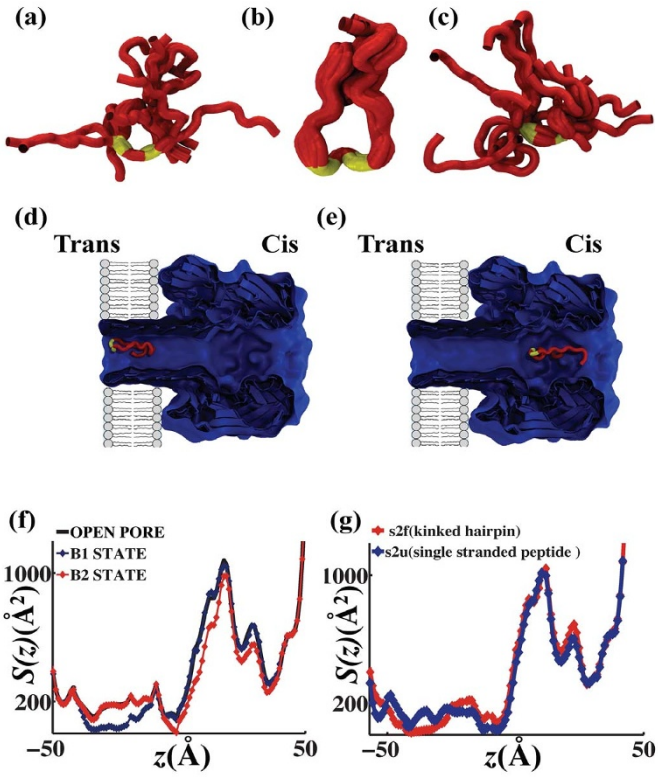


**Figure 2 | Simulations of peptide translocation ensembles.** Conformations of (a) free peptide, (b) peptide within the β-barrel (representative B1 state) and (c) peptide within the vestibule (representative B2 state) are shown. A typical MD simulation trajectory of peptide during trans-cis translocation of peptide with snapshots at two states (d) B1 state and (e) B2 state. The cross sectional areas used to compute the current signals during translocation: (f) a comparison of the open pore cross-section with the cross-sectional area of the pore when the peptide is in the β-barrel (B1) and in the vestibule (B2); (g) the cross sectional area and hence current signatures would be different also for a kinked hairpin peptide vs. a linear single stranded peptide (see Fig. S5, SI).

as function of conformation dynamics of the peptide during atomistic simulation (Fig. S5, panel b) at a constant neutral pH, follow closely being in the range of 0.24–0.38 for B1 and 0.49–0.70 for B2. This further supports the measured intermediates and provided atomic details of putative peptide conformational ensembles within the β-barrel and vestibule.

A further task was to rationalize the data on the average time values corresponding to consecutive peptide-induced blockage events ($\tau_{ON}$) recorded at variable pH values. To account for why does the peptide association rate to the pore ($rate_{on} = \tau_{on}^{-1}$) dramatically decrease with lowering the pH (Fig. 3, panel a), we note that at the mouth end of the protein β-barrel, pointing to the trans side buffer lies a charged 7-fold symmetric ring composed of 14 aspartic acids (D127 and D128) and 7 lysines (K131) from the seven protein monomers, which at acidic pH assumes a net positive charge[56], that may constitute an electrostatic barrier for the incoming positively charged peptides. That is, at low pH values, the local concentration of peptides near the β-barrel mouth lowers as a direct consequence of the repulsive interactions between the peptides (whose net positive charge remains un-affected by the pH drop) and the mouth, leading to a corresponding decrease in the peptide association rate to the β-barrel (Fig. 3, panel a).

The next issue was to unravel the mechanism leading to the pH-dependent peptide dynamics through the vestibule, reflected by an increase in the duration ($\tau_{off}\ B_2$) of the lower blockage level $B_2$ at acidic pH values of the buffer (Fig. 3, panel b). A statistical analysis of the vestibule translocation rates ($rate_{off}\ B_2 = \tau_{off}\ B_2^{-1}$) as a function of pH and of the potential applied across the membrane showed that lowering the pH leads to a considerable decrease of the rate of vestibule passage, suggesting that the dynamics and possibly the mechanism of peptide translocation are critically dependent upon buffer acidity.

One possibility to rationalize this observation lies in the pH tuning effect on the net charge of the α-HL vestibule, which becomes positively charged at acidic pH's, as the protonation of D13, D2, D4, D227 on each of the seven monomers of the α - HL homo-heptamer leads to un-compensated positive charge on residues K8, R56, R104, K154 (Fig. S6, SI). Therefore, to explain the effect of pH on peptide translocation through the protein, two putative mechanisms may be invoked: (i) the non-specific, long-range electrostatic repulsion between the peptide and the protein inner surface, and (ii) the interplay between the electro-osmotic flow through the anion-selective protein and the electrophoretic motion of the peptide along the electric field within the protein pore. Although at 2 M KCl solution, the Debye length is $\kappa^{-1} \sim 1.9$ Å, which is low value relative to the average diameter of the vestibule (46 Å), we cannot completely rule out the existence of a disordered energy landscape as the peptide moves along the pore, caused by the heterogeneity in the charge distribution all along the protein at various pH values. In addition to this, the microscopic understanding of all forces acting on the translocating peptide is further complicated by possible peptide adsorption processes at the mouth and inner surface of the protein pore, which may interfere with the electro-osmotic effects and non-specific electrostatic interactions between the peptide and the pore[57,58]. Such pH-dependent, non-specific electrostatic interactions between the peptide and the inner surface of the pore, may be embodied in a distinct contribution to the net value of peptide mobility through α-HL. To provide a mechanistic description of the pH-dependent peptide translocation through α-HL within the simplest analytical model, we focused herein on the second mechanism, whereby the electro-osmotic flow of water within the protein vestibule adds up as a supplementary contribution, i.e. the convective velocity to peptide transport, thus altering the absolute velocity of the peptide measured with respect to the protein walls and its translocation dynamics. The low-pH augmented overall positive charge of the α-HL inner surface[56], which contributes to an enhanced anionic selectivity of the protein nanopore and electro-osmotic flow of the fluid, lends further support to the present approach. In support to this mechanism, it should be noted that by lowering the pH buffer below 5 results in almost doubling of the protein anion-selectivity as compared to neutral pH ($P_{K^+}/P_{Cl^-} = 0.44$ at pH 4.4 and $P_{K^+}/P_{Cl^-} = 0.86$ at pH 7.1, data not shown). Thus, in the presence of an applied positive potential in the trans side of the membrane, the cis-to-trans oriented motion of water associated to the enhanced transport of anions across the pore, results in an appreciable influence of the drift velocity of the translocating peptide through the protein vestibule (Fig. 4). With direct relevance to the present work and as an additional support for this model, most recently it was demonstrated the possibility of controlling the electro-osmotic flow through a nanopore by modulating the surface charge, which in turn directly affected the speed of translocating molecules[59].

Assuming negligible contributions from pressure gradients, the drift velocity of a peptide in the electric field along the protein vestibule is the vector sum of the electrophoretic and electro-osmotic components. Because the protein is anion selective, such that the positively charged peptide moves trans-to-cis, opposite to the net flow of water carried by cis-to-trans moving anions, electro-osmotic water flow opposes electrophoresis and the drift velocity of a peptide moving along the electric field lines, in the trans to cis direction within the protein vestibule can be written as (see SI):

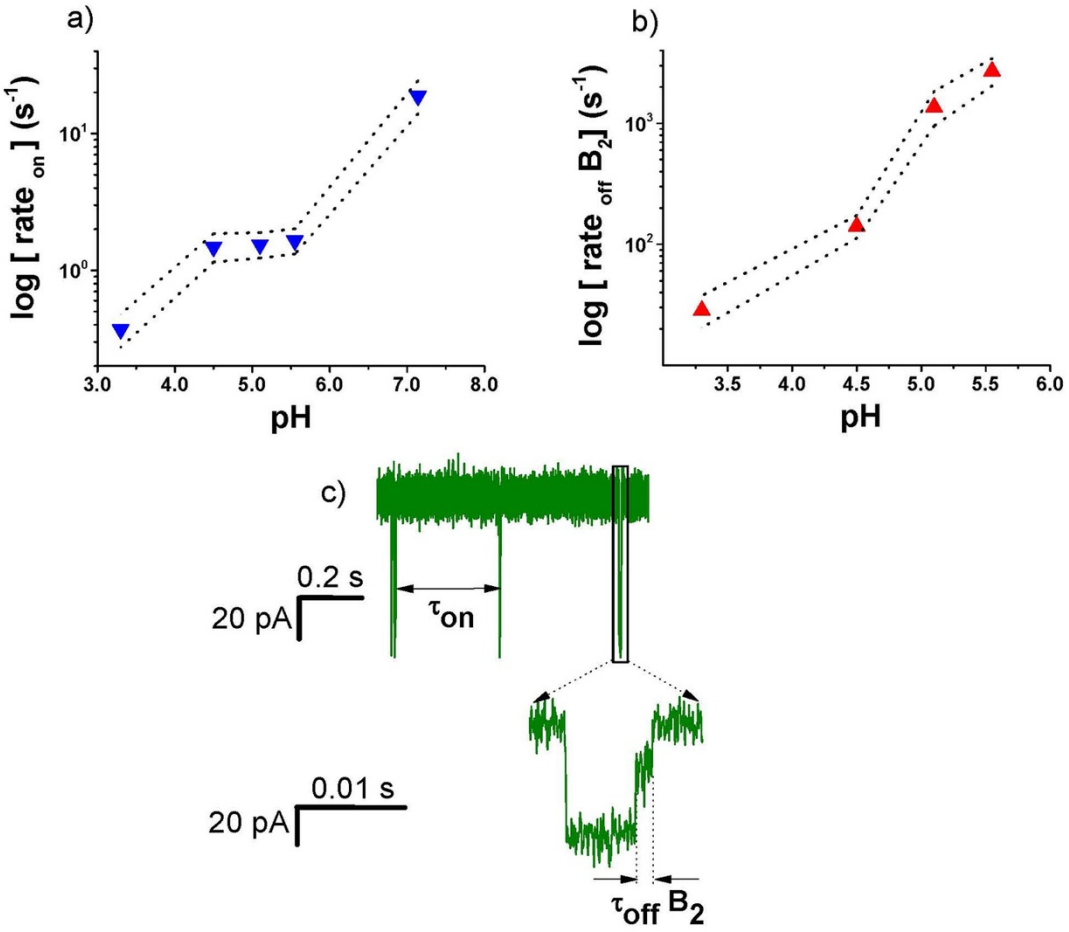


**Figure 3 | (a) pH-dependence of peptide association rate to the pore β-barrel ($rate_{on}$) from exponentially-distributed time intervals between consecutive blockage events ($\tau_{on}$) (at +50 mV) (b) pH-dependence of dissociation rate from vestibule from average dwell-time values in the $B_2$ state ($\tau_{off}B_2$).** Dotted lines in (a) and (b) represent the 95% confidence domain for $rate_{on}$ and $rate_{off}B_2$ values, respectively. (c) Typical segment of current trace at +50 mV for 30 μM peptide added on the trans-side of the membrane, at pH = 5.1, to pinpoint the representative time intervals associated to peptide association with the open protein pore ($\tau_{on}$) and translocation across the protein vestibule ($\tau_{off}$ $B_2$).

$$v_{drift} = v_{electrophoretic} - v_{electroosmotic} = \mu\frac{\Delta V}{l_{pore}} - \frac{(P_{Cl-} - P_{K+})}{(P_{Cl-} + P_{K+})}N_h I \Big/ \left(|e^-|S_{pore}[H_2O]\right) \quad (1)$$

with $S_{pore}$ as the average cross-sectional area of the α-HL vestibule, μ the electrophoretic mobility of the peptide within the vestibule, $N_h$ the number of water molecules associated with each mobile ion, $[H_2O]$ the water concentration, $I$ the net electric current transported while a peptide resides within the vestibule (i.e., corresponding to the $B_2$ sub-state), $e^-$ the electronic charge, $P_{K+}$ and $P_{Cl-}$ the ionic permeabilities and $\Delta V/l_{pore}$ the electric field. Therefore, as the pore augments its anion selectivity ($P(Cl-)/P(K+) \gg 1$), electro-osmosis increases and the drift velocity decreases. Thus, controlling the balance between the electrostatic and electro-osmotic forces is emerging as a useful strategy to trap and identify translocating molecules (examples are individual nanoparticles[60] or DNA[61]). An interesting limit exists in which electro-osmosis compensates electrophoresis ($v_{drift} = 0$), so that the peptide stalls within the pore. To probe this limit, we carried out experiments at such lower pH that the anionic selectivity of the α-HL protein and therefore the electroosmotic flow were substantially augmented. Under such circumstances a peptide captured by the protein β-barrel would likely bounce back and forth within the pore before its release on either side. Our data supported this hypothesis (Fig. S2). Data collected at pH = 3.3 and pH = 2.2 show that peptide capture in the β-barrel ($B_1$ blockage), is followed by the $B_2$ sub-state when the peptide migrates to the vestibule, as expected, but, unlike data collected at less acidic pH's, a peptide confined within the vestibule ($B_2$ sub-state) did not get released from the pore. Instead, the $B_1$ blockage sub-state ensued again, indicating movement backwards to the β-barrel (Fig. S2, panel a). Only after several back-and-forth transitions between the $B_1$ and $B_2$ sub-states, the pore entered the 'open' sub-state (O), and the peptide was released. We note that such reversible $O \rightarrow B_1 \leftrightarrow B_2 \rightarrow O$ transitions were also observed in ~4% of the events studied at pH = 4.5, but they became significantly prevalent at the lower pH's, so that at a pH = 3.3 such reversible transitions appear in ~22% of cases. Upon decreasing the pH furthermore (pH = 2.2), the peptide even reversed its direction: as shown in a representative trace, after an $O \rightarrow B_1 \rightarrow B_2 \rightarrow O$ sequence of events, the peptide immediately re-entered the vestibule, getting trapped again in the $B_2$ sub-state (Fig. S2, panel b). We posit that despite being released on the cis side of the membrane, the electro-osmotic flow manifested on the immediate vicinity of the protein vestibule at such low pH's serves as a trap for the peptide, which is therefore guided backwards into the pore, against the electric field across it. Only after several such reversible transitions ($O \leftrightarrow B_2$), the peptide managed to fully disengage from the electro-osmotic trap and dissociate from the protein (Fig. S2, panel b). In support of this scenario anion selectivity at pH = 2.84 equals $P_-(Cl-)/P_-(K+) = 3.6$, so that Eq. (1) with $\Delta V$ = +50 mV and with a diffusion coefficient $D = 1.5*10^{-12}$ $m^2 s^{-1}$ (see below) predicts a negative value of the peptide drift velocity $v_{drift} \sim -1*10^3$ μm $s^{-1}$,

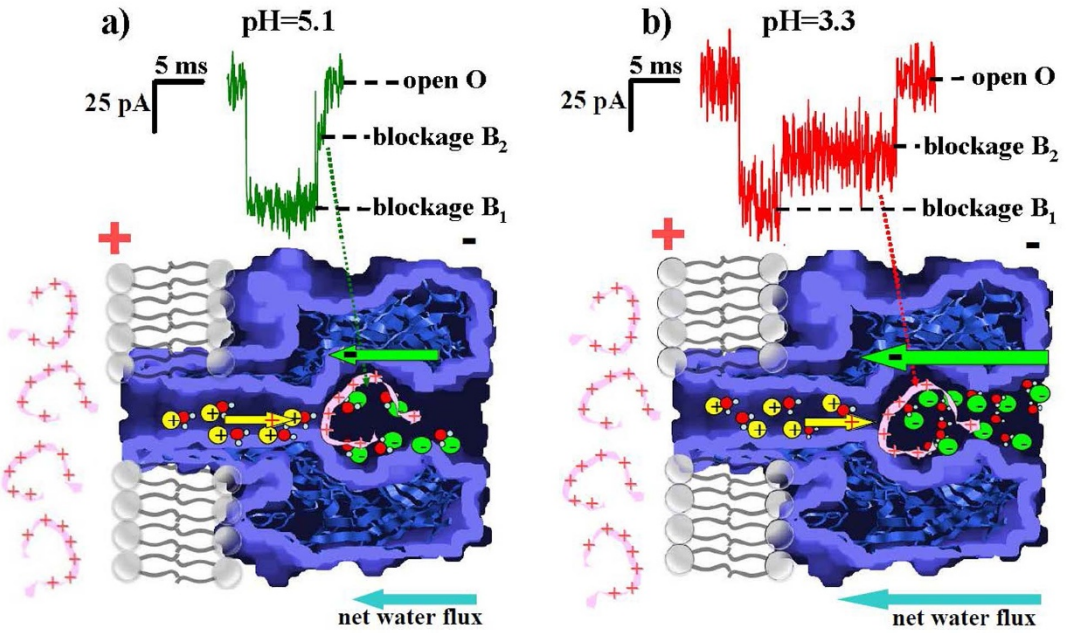


**Figure 4 | Schematic representation of pH-augmented electro-osmotic braking, i.e., anion selectivity of the α-HL pore as means to slow-down trans-to-cis peptide passage.** At acidic pH and positive potential on the trans side, the flux of anions transported cis-to-trans is higher than that of cations, transported oppositely, leading to a net water flux in the cis-to-trans pore direction. The electro-osmotic water flux translates into an increased duration of the time spent by the peptide in the vestibule during its journey from trans to cis under the positive potential; based on acidic pH-augmented anion selectivity of α-HL, this phenomenon is more prevalent at pH = 3.3 (panel b) than pH = 5.1 (panel a).

i.e., opposite the electrophoretic drift. The peptide therefore can move backwardly against the electric field, giving rise to chain of molecular events described above. To explain how the peptide can "sense" the electro-osmotic flow outside the αHL pore, and gives rise to B2 ↔ O sequence of events, one may note that in a recent paper, authors demonstrated that the electro-osmotic flow inside the nanopore is able to generate a hydrodynamic flow field in the vicinity of the pore comparable in size with the radius of gyration of the transported polymer[62]. Applied to our case, it is thus conceivable that the velocity gradient of the water flow near the *cis* mouth of the nanopore at acidic pH, may give rise to an adsorbing region able to funnel the peptide back into the α-HL vestibule.

We now focus on the control of time sequencing of state-to state dynamics. To correlate quantitatively the experimentally observed lengthening of translocation time values of peptide with the drop in the buffer pH, we next modeled the sojourn time of the charged peptide as the first passage time for one-dimensional diffusion in a constant electric field and under the influence of the electro-osmotic flow of water. As previously demonstrated[57], and taking into consideration that in our situation the net drift velocity of the peptide is given by Eq. (1), the distribution of peptide sojourn times into the protein vestibule is described by the probability density function[63] of the type $p(t) = \left((v_{\mathrm{drift}}t + l_{\mathrm{vestibule}})\exp\left[-(l_{\mathrm{vestibule}} - v_{\mathrm{drift}}t)^2/4Dt\right]\right)/\left(2t\sqrt{4D\pi t}\right)$, where $l_{\mathrm{vestibule}}$ represents the vestibule length, $D$ the diffusion coefficient of the peptide within the vestibule, and the drift velocity of the peptide ($v_{\mathrm{drift}}$) accounts for both its interaction with the electric driving force and the electro-osmotic flow of water. This probability distribution yields an expression for the average time spent in the vestibule:

$$\langle t_{\mathrm{off}}\rangle = \frac{1}{\mathrm{rate}_{\mathrm{off}}\mathrm{B}_2} = \int_0^{\infty} \frac{t(v_{\mathrm{drift}}t + l_{\mathrm{vestibule}})e^{\left[-\frac{(l_{\mathrm{vestibule}} - v_{\mathrm{drift}}t)^2}{4Dt}\right]}}{2t\sqrt{4D\pi t}}dt = \frac{v_{\mathrm{drift}}l_{\mathrm{vestibule}} + D}{{v_{\mathrm{drift}}}^2} \quad (2)$$

From a mechanistic point of view, the expression for $\langle t_{\mathrm{off}}\rangle$ agrees well with data in Fig. 4: at low pH, the enhanced anion selectivity of the protein will reflect in part in an augmented electro-osmotic water flux, that eventually lengthens the sojourn of the peptide in the protein vestibule, before its release to the cis side of the membrane. This is in further agreement with previous results showing that electro-osmosis plays crucial roles in protein translocation across nanopores, which in certain cases may occur oppositely to what simple electrostatics would indicate[64].

The voltage-dependence of the dissociation rate corresponding to the lower blockage level ($B_2$) associated to the peptide translocation across the protein vestibule is shown in Fig. 5, panel d. Based on the experimental evidence presented herein, we conjecture that, at low pH values, the kinetics of peptide translocation is dominated by the slowest translocation step, which appears to be the peptide movement along the protein vestibule, and a larger potential drop ensues a correspondingly shorter translocation time as embodied by expression[2]. Therefore, supplementary to previous data reporting the voltage-dependence of peptide translocation through α - HL pores[19,65], estimated near neutral pH, we posit that besides the electric field, the electro-osmotic force contributes essentially to peptide dynamics within α-HL at acidic pH's. The rather restrictive topology of the α - HL β-barrel imposes peptide confinement, resulting in large conformational entropy and enthalpy changes that lead to a barrier for peptide displacement under the applied potential. Translocation is thereby governed by a rate obeying classical Kramers theory, depending exponentially on voltage. At acidic pH, as experimentally demonstrated herein, the peptide translocation is dominated by its journey through the pore vestibule which given its larger size, does not pose an overwhelmingly entropic or enthalpic barrier to translocation, and peptide release to the cis side of the membrane reflects mainly a diffusive motion biased by the applied potential, which can be addressed by invoking the drift-diffusion formalism.

Due to the fact that the blockage amplitude of sub-state $B_2$ depends linearly on the applied potential (Fig. 5, panel e), suggesting the absence of a reduction in the excluded volume inside the protein, we ruled out the possibility that the peptide stretches in the vestibule

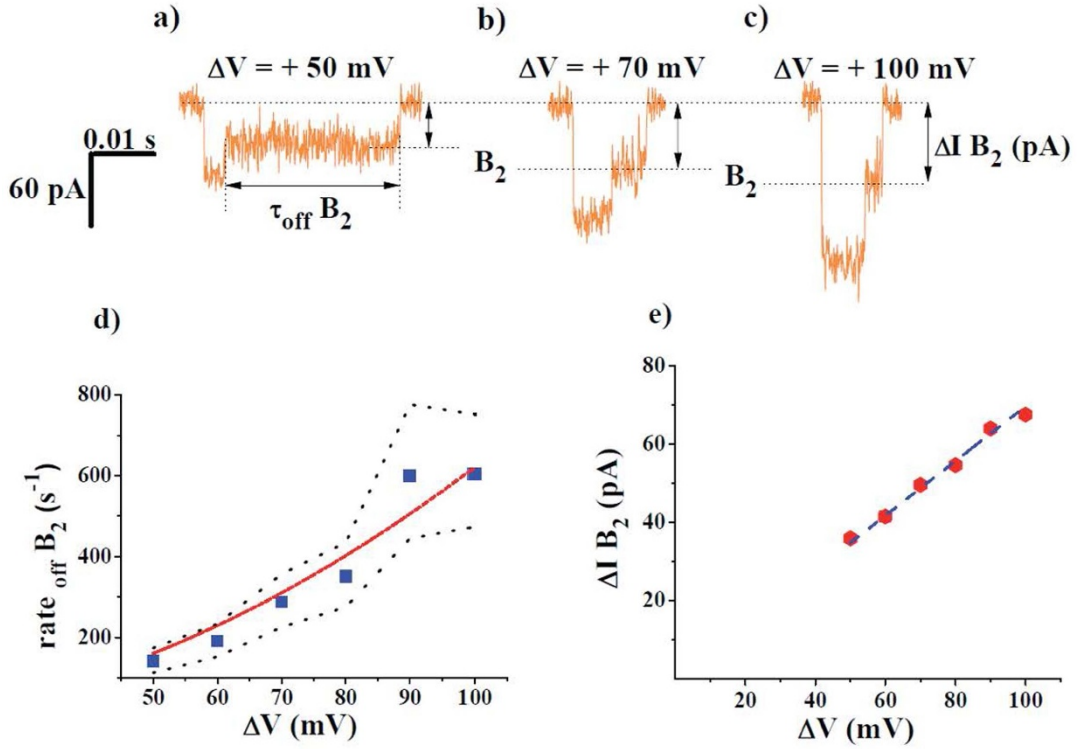


**Figure 5 | (a–c) Selected segments of voltage-dependence of peptide sojourn in $B_2$, quantified via dwell-time ($\tau_{off}$ $B_2$), as well as amplitude of pore blockage induced by peptide trapping within the vestibule ($\Delta I_{B2}$) relative to open-pore current (pH = 4.5).** Statistical analysis yielded voltage-dependence of the rate of peptide exiting the $B_2$ sub-state ($rate_{off}B_2$; panel d) and the I-ΔV dependence of $\Delta I_{B2}$ measured at pH = 4.5 (panel e). Dotted lines in (d) represent 95% confidence domain for $rate_{off}B_2$. Data in (d) were non-linearly fitted (dashed-line) to estimate the peptide diffusion coefficient *D* within the vestibule.

under the applied potential. This means that the peptide assumes a relatively stable conformation during translocation through the vestibule and therefore the diffusion coefficient of the peptide moving in the vestibule remains invariant within the range of the applied potentials. Furthermore, and as we show in Fig. S7, the association rate reflecting the interaction of a single CAMA P6 peptide with the α-HL protein ($O \rightarrow B_1$, $rate_{on}$, ▼) (panel a), and the rate characterizing the $B_1 \rightarrow B_2$ transition ($rate_{off}B_1$, ◆) (panel b), estimated at pH = 4.5 also display a voltage dependent behavior. We posit that the voltage-dependent capture rate of the peptide (the $O \rightarrow B_1$ transitions) is indicative of an enhanced peptide-protein association constant at increased transmembrane potentials, resulting most likely from the fact that the applied potential lowers the height of this *trans* energy barrier of peptide partitioning into the α-HL β-barrel[19]. Surprisingly however, the rate characterizing the $B_1 \rightarrow B_2$ transition ($rate_{off}B_1$) decreases as the transmembrane potential is enhanced, paradoxically displaying an opposite behavior to that of the rate characterizing the $B_2 \rightarrow O$ transition ($rate_{off}B_2$) (Fig. 5, panel d). That is, one would expect that as the transmembrane potential increases, the net value of the electrophoretic speed component increases (see expression 9, SI), and the overall drift velocity of the peptide across the α-HL's β-barrel increases correspondingly (see expression 1). To rationalize the experimental observation, we suggest that in the more confined volume of the protein's β-barrel, the electro-osmotic speed component increases more steeply with the transmembrane potential than the electrophoretic speed of the peptide, which tends to drive the peptide towards the vestibule. This may be due to a voltage-mediated reduction in electrophoretic mobility of the peptide within the β-barrel, and a similar phenomenon was reported recently[38]. In addition, it may be that an increased transmembrane potential could lead to a lengthening of the time needed for the peptide to search randomly for an optimal orientation that would facilitate translocation across the constriction region, which would rate-limit the peptide translocation along the β-barrel. Undoubtedly, further experiments and computational modeling are required to resolve the origin of this seemingly anomalous dynamics of the peptide inside the β-barrel, at acidic pH's.

With experimental parameter values (see SI) we employed Eq. (2) to estimate the diffusion coefficient *D* of the peptide in the vestibule at pH = 4.5. By non-linear fitting of data in Fig. 5(d) with Eq.(2), (i.e., the $rate_{off}$ $B_2$ vs. $\Delta V$ dependency), we arrived at $D = 1.5*10^{-12}$ $m^2s^{-1}$. Existing data on diffusion of peptide with comparable size *in water* suggest a value between $D = 5*10^{-10}$ $m^2$ $s^{-1}$ ÷ $10^{-9}$ $m^2$ $s^{-1}$ [66,67]. Our result, placing the diffusion coefficient in the vestibule two orders of magnitude lower, reflects the restricted movement of the confined peptide within a nanoscopic volume, mediated by local interactions with the protein inner walls (involved in the so-called internal friction[68]) as opposed to the free peptide diffusion in the bulk. For comparison, a similarly sized peptide in a buffer slightly more viscous that water, was measured to have $D = 2.4*10^{-12}$ $m^2$ $s^{-1}$ [69].

It should be noted that if electro-osmotic effects were negligible, i.e., if the second term in Eq. (1) was set to zero, the non-linear fit of data in Fig. 5, panel (d) with Eq. (2), in which the average value of the peptide drift speed within the protein vestibule would write simply as $v_{drift} = \mu\Delta V/l_{pore}$, would result in a value of the peptide diffusion coefficient $D \sim 10^{-15}$ $m^2$ $s^{-1}$, which is at least three order of magnitude less than values reported in the literature (vide supra). Such a diffusion coefficient is unrealistically slow also when invoking the Stokes-Einstein equation ($D = kT/6\pi\eta r$) for the diffusion of the peptide viewed as a spherical particle of radius $r = \sqrt[3]{(3/4\pi)\delta_{volume}}$, where $\delta_{volume}$ represents the peptide's effective volume. In the protein vestibule where the apparent viscosity of water was estimated at $\eta = 0.2$ Pa s (vide infra), a diffusion coefficient of $D \sim 10^{-15}$ $m^2$ $s^{-1}$

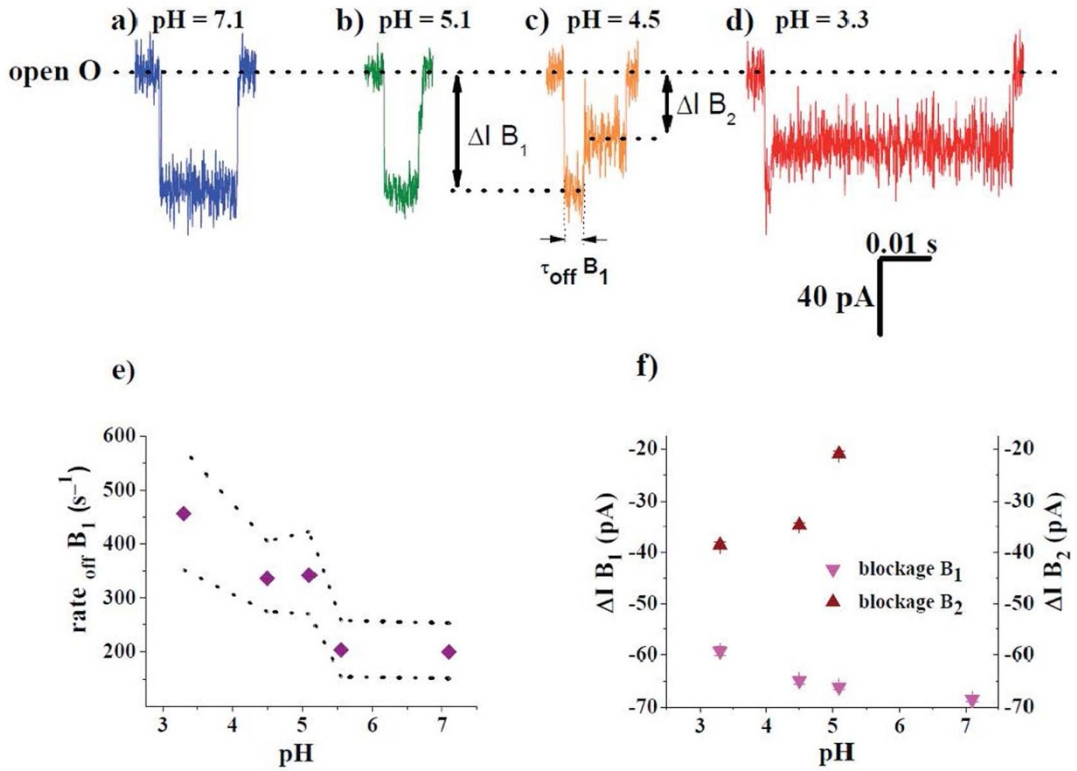


**Figure 6 | pH-dependence of translocation kinetics and blockage amplitudes.** Representative current traces in (a)–(d) same as in Fig. 1. Statistical analysis quantified hereafter in terms of reaction rates (panel e) shows a definite increase in the dissociation rate ($rate_{off}\ B_1$) of the peptide from the β-barrel for more acidic pH values, as the peptide moves toward the protein vestibule to later exit on the cis side. Dotted lines represent the 95% confidence domain for the $rate_{off}\ B_1$. Panel f quantifies the pH-dependence of the relative current blockage ($\Delta I_{block}$) induced by a peptide corresponding to the two distinct blockages, i.e., in sub-states $B_1$ and $B_2$.

would result in $\delta_{volume} \sim 5\ \mu m^3$, which is unrealistically high for a 20 amino-acid long peptide as clearly such a volume does not fit the pore.

We note that control experiments carried out at a basic pH (pH = 9.17), convincingly showed the absence of the blockage sub-state $B_2$, and the scatter plot of dwell time vs. relative blockage amplitude of blockage events ($\Delta I_{block} = I_{B1} - I_O$) detected at this pH revealed only the $B_1$ sub-state (Fig. S8). This observation can be rationalized through the quasi-absent anion selectivity at neutral-to-basic pH's[70] which, with relevance to our experiments, reflects into a much decrease electro-osmotic force acting oppositely to peptide movement thus strengthening further the role played by the electro-osmotic flow in slowing down the peptide motion through the vestibule.

To further probe the origin of the slow-down, we employed other synthesized peptide constructs, termed CAMA P1 (KWKLFKKIGIGKHFLSAKKF-NH2) and CAMA P5 (KWKHLKKIGIGKHFLSAKKF-NH2), that contained one (CAMA P1) and two histidines (CAMA P5), respectively (see also Table S2). In doing so, we ensured that at mildly acidic pH values (e.g., pH = 4.5), and below the histidine's pKa measured in solution (pKa ~ 6), the net charge on these peptides will be greater by one (CAMA P1; effective charge $\sim 9|e^-|$at pH = 4.5) and respectively two (CAMA P5; effective charge $\sim 10|e^-|$at pH = 4.5) electron charges, by comparison to CAMA P6 (effective charge $\sim 8|e^-|$at pH = 4.5), see Table S2. We reasoned that due to their close geometrical size and hydrophilicity, the dwell time of CAMA P5 peptide within the α-HL vestibule measured at pH = 4.5, under the influence of a similar positive potential and electro-osmotic force, would be shortest as compared to CAMA P1 and CAMA P6 – in this order – as a direct consequence of its higher positive charge. As demonstrated by results shown in Fig. S9, it is clear that $\tau_{off}\ B_2$ is shortest for the case of CAMA P5 peptide (Fig. S9, panel c), as compared to CAMA P1 (Fig. S9, panel b) and CAMA P6 (Fig. S9, panel a). The calculated dissociation rate values $rate_{off}\ B_2$ associated to the release of the three distinct peptides from the α-HL vestibule at pH = 4.5 ($rate_{off}\ B_2$ (CAMA P5) = 917.4 ± 182.8 $s^{-1}$; $rate_{off}\ B_2$ (CAMA P1) = 276.2 ± 37.5 $s^{-1}$; $rate_{off}\ B_2$ (CAMA P6) = 141.4 ± 15.2 $s^{-1}$). To partially account for the larger mobility of CAMA P5 and CAMA P1 peptides as compared to CAMA P6, we do not rule out an additional pH-induced change in peptide folding mechanism, due to the partial protonation of histidine residues at acidic pH values[71].

A seeming puzzle was the anomalously small residence times of the peptide within the protein β-barrel at acidic pH values (Fig. 6). One would expect that, as for the peptide moving within the vestibule (vide supra), an augmented electro-osmotic flow manifested at low pH would impede peptide movement across the β-barrel as well, and therefore that the translocation rate describing the peptide escape from the β-barrel towards the vestibule would decrease. Nevertheless, our data demonstrated the opposite tendency: peptides displayed a shorter residence time within the β-barrel at acidic pH values (Fig. 6, panels a–e). It may be possible that acidic pH values may trigger conformational changes in the peptide that lead to its increased mechanical mobility, or that reduce the activation barrier for moving across the pore constriction towards the vestibule. The mechanistic origin of this may stem from the net water flux that, within the β-barrel, can tug on the peptide to elongate it, thus facilitating the peptide threading through. This reconciles both the experimental observation that the β-barrel blockage ($\Delta I\ B_1$) is smaller at low pH (Fig. 6, panel f), pointing to a progressive, pH-induced decrease of the excluded volume within the β-barrel, and the simulation data, that shows larger cross section area available for the current upon passing an unfolded single stranded peptide vs. a kinked hairpin (Fig. 2, f–g).

While at constant pH we observed no change in peptide volume vs. applied potential (see Fig. 5, panel e), such a change was observed in volume vs. pH dependences (Fig. 6, panel f and discussion in SI). This indicated that elevated values of the electro-osmotic flux acting collectively and oppositely to the electrophoretic force create local forces that can induce gradual changes in the folded volume of the confined peptide, along the axis of the protein pore. This effectively lowers the drag by a reduction in the hydrodynamic cross section of the peptide and explains the shortening of the β-barrel sojourn with pH. Independently from our estimate of $D = 10^{-12}$ $m^2$ $s^{-1}$ (Fig. 5, panel d), we also estimated (see SI) the diffusion coefficient from the blocking volume of the peptide (approx. 4.13 $nm^3$) via a Stokes-Einstein's relationship, leading to an unrealistically high D (approx. $10^{-10}$ $m^2$ $s^{-1}$). Bringing D to the true estimate of $10^{-12}$ $m^2$ $s^{-1}$ led to value of the water viscosity $\eta = 0.2$ Pa s, in agreement with anomalous viscosity of water in nano-confined volumes[72,73]. Taken together, data presented in Fig. 3b and Fig. 6e reveal yet another insight. The rate limiting step for peptide release from the pore is dictated by the peptide's longest residence in one of the two spatially distinct regions of the pore, i.e., either the β-barrel or the vestibule, which in turn depends on the pH. That is, at pH = 3.3, the experimentally inferred reaction rate corresponding to the peptide traversing the pore's β-barrel ($rate_{off}$ $B_1$) is at least one order of magnitude higher than that associated to the peptide exiting the pore's vestibule ($rate_{off}$ $B_2$) (pH = 3.3; $rate_{off}$ $B_1$ = 456.46 ± 55.4 $s^{-1}$ and $rate_{off}$ $B_2$ = 28.38 ± 4.28 $s^{-1}$), whereas an opposite tendency is seen at a higher pH (pH = 5.5; $rate_{off}$ $B_1$ = 203.05 ± 25.9 $s^{-1}$ and $rate_{off}$ $B_2$ = 2.6*$10^3$ ± 3.5*$10^2$ $s^{-1}$). Moreover, towards neutral and basic pH values, while peptide's residence in the β-barrel steadily blocks the current, peptide passage through the vestibule becomes so fast that it evades detection (see Fig. 1, panel a and Fig. S8). The fact that the journey of a peptide through the α-HL pore is limited in kinetic terms by the distinct pore compartments within the diffusive pathway may have far reaching consequences for the task of devising more efficient α-HL protein-based architectures to be used in molecular recognition studies of peptides or other macromolecules.

## Discussion

In this work we have demonstrated that peptide capture and translocation kinetics through the native α-HL protein can be readily tuned by varying the buffer pH. Our approach provides a unique look to visualize sequentially the peptide translocation process, as it proceeds through the β-barrel and vestibule of the protein. Through analysis of parameters such as current blockage induced by peptide within the protein pore and residence time in various domains of the diffusing pathway, we discovered that peptide dynamics through the channel is largely determined by the overall charge within the electro-diffusion pathway, and that the electro-osmotic flow imposes a marked difference on peptide translocation particularly at low pH values, slowing down the peptide drift velocity along the vestibule region. An intriguing consequence of our studies is that the mechanism of peptide dynamics within the α-HL protein is amenable to further development at low pH values in particular, through the fact that when acting oppositely, the lumped force stemming from the low pH-enhanced electro-osmotic flux and the electrophoretic force, can induce gradual changes of the folding of a β-barrel-confined peptide, resulting in an augmented propensity of the peptide for moving across the protein constriction barrier towards the vestibule. We further suggest the manifestation of distinct spatially-localized peptide-α-HL protein interaction sites, which rate-limit the peptide journey through the α-HL pore depending on the pH, in the sense that, for example, peptide translocation kinetics through the α-HL pore at low pH values is set by the peptide journey across the protein's vestibule region. Our data highlights the immense potential offered by the single-protein-based approach towards identifying consecutive reactions steps associated to peptide binding within distinct regions within nanopores, characterized by reaction rates differing by orders of magnitude, impossible to detect from ensemble-based measurements.

These results demonstrate the facile possibility to control and reduce the translocation of guest macromolecules between the inner compartments of the α-HL protein pore rendering it discontinuous along the permeation pathway, thus paving the way to a more accurate exploration of macromolecules-induced blockage depths. With the implication of complimentary single-molecule tools, such as atomic force microscopy and optical tweezers, and working in conjunction with supra-molecular guests as a way to produce protein pores with internal topologies possessing particular physico-chemical properties, or employing tailored enzyme-driven translocation approaches, such model systems may be refined, to probe with improved spatio-temporal resolution the folding and translocation of biological polymers.

Given the complexity of the biological and physical aspects related to a complete exploration and description of local forces that alter the peptide dynamics within the pore at various pH values, whereby the charged state of crucial residues pointing towards the inner volume of the α-HL changes with solution acidity, single point mutagenesis on the α-HL pore remains a tool of choice in order to provide direct evidence of residues relevant for peptide translocation. We therefore presented a proof-of-concept system which could be refined and further embedded in integrated single-molecule platforms that allow controllable stalling and releasing of the pore-captured macromolecules, and control the kinetic behavior and folding of peptides within nano-volumes.

## Methods

**Peptide synthesis.** The peptides were synthesized using the solid phase method with Fmoc (9-fluorenyl-methoxycarbonyl)-chemistry[74,75]. Peptide purification was then carried out using preparative HPLC on a C18 reverse-phase column. The amino acid compositions of the purified peptides were confirmed using an amino acid analyzer (HITACHI 8500A, Japan). The molecular weights of the synthetic peptides were determined using a matrix-assisted laser desorption ionization (MALDI) mass spectrometer (see Table S3 and Fig. S10 for mass analysis of the peptides).

**Electrophysiology.** Single molecule electrophysiology experiments were performed as previously described[20,65]. Planar lipid membranes made of 1,2-diphytanoyl-sn-glycerophosphocholine (Avanti Polar Lipids, Alabaster, AL) were obtained using the Montal–Mueller technique[76,26] across a 1 : 10 hexadecane/pentane (HPLC-grade, Sigma–Aldrich, Germany) pretreated, ~120 μm in diameter orifice punctured on a 25 μm-thick Teflon film (Goodfellow, Malvern, MA) that separated the *cis* (grounded) and *trans* chambers of the recording cell. The electrolyte used in both chambers contained 2 M KCl buffered in 10 mM HEPES (Sigma−Aldrich, Germany) for experiments performed at neutral pH = 7.1, or 5 mM MES (Sigma−Aldrich, Germany) for experiments carried out at mildly acidic pH values (pH = 3.3, 4.5, 5.1). All reagents were of molecular biology purity. After obtaining a mechanically stable lipid bilayer, ~0.5−2 μL of α-hemolysin (α-HL) (Sigma−Aldrich, Germany) were added from a monomeric stock solution made in 0.5 M KCl, to the grounded, cis chamber, under continuous stirring for about 5–10 minutes. Once the successful membrane insertion of a single α-HL heptamer was attained, and depending on the particular experiment, either CAMA P6, CAMA P1 **or** CAMA P5 peptide was introduced in trans chamber at a bulk concentration of 30 μM, from a 1 mM stock solution made in distilled water. To alleviate electromagnetic and mechanic interference, the bilayer chamber was housed in a Faraday cage (Warner Instruments, U.S.A), and placed on the top of a vibration-free platform (BenchMate 2210, Warner Instruments, U.S.A). All experiments were carried out at room temperature of ~23°C. Electric currents mediated by a single α-HL protein pore immobilized in a lipid membrane, in the absence or presence of peptides, were detected and amplified via a Multi Clamp 700B amplifier (Molecular Devices, U.S.A) set to the voltage-clamp mode, and filtered at 30 kHz with the built-in low-pass Bessel filter. Data acquisition was performed with a NI 6251 acquisition board (National Instruments, U.S.A) at a sampling frequency of 80 kHz, with customized routines written in the LabVIEW 8.20(National Instruments, U.S.A) environment. The statistical analysis on the relative blockage amplitudes induced by peptides on the electric current through a single α-HL protein, as well as the frequency and duration of the peptides-induced current blockades were analyzed within the statistics of exponentially distributed events, as previously described[77]. In short, we approached the statistical inference of rate constants using an alternative procedure to dwell-time histograms, as proposed originally in a previous work[77], whereby the average time values separating two consecutive blockage events and average blocked time were employed to derive association and dissociation rate constants describing the reversible interaction between peptides and the α-HL protein. The inverse of

average time values corresponding to the inter-event blockage intervals ($\tau_{on}$) and various peptide-induced blockage levels ($\tau_{off}$), provided quantitative estimations of the association ($rate_{on}$) and dissociation ($rate_{off}$) reaction rates characterizing the α-HL - peptide reversible interaction. As indicated in Fig. S11, representative histograms of time intervals associated to the $B_1 \rightarrow B_2$ transition ($\tau_{off}B_1$) and $B_2 \rightarrow O$ transition ($\tau_{off}B_2$), respectively, collected at various acidities (i.e., pH = 7.1, pH = 4.5 and pH = 3.3) and an applied transmembrane potential $\Delta V = +50$ mV, were best fitted with a decaying mono-exponential function ($y \sim \exp(-t/\tau_{off})$). This in turn indicates the existence of only one type of peptide population interacting with the protein pore, so that we are bound to believe that our system does not discriminate between the orientation of the peptide in the pore entering with either the C- or N-terminal. Data graphing and statistics were mainly done with the help of the Origin6 (Origin Lab, U.S.A) and pClamp 6.03 (Axon Instruments, U.S.A) software. At least three independent experiments were carried out in order to arrive at the numerical estimates reported herein.

**Simulation methods.** Peptide sequence, CAMA P6 (KWKLFKKIGIGKFLQSAKKF) is translocated across alpha-hemolysin pore from the trans - to cis - end by using electric field corresponding to a trans-membrane voltage of +90 mV. The electric field is calculated from the applied trans-membrane voltage through the extent of the system along the z-axis, given by, $V = -EL_z$. The peptide coordinates were generated in PYMOL, minimized for 5000 steps using a combination of Steepest descent method and adopted basis Newton Raphson method followed by heating to 300 K with constraints on the heavy atoms and subsequent equilibration at 300 K by slowly removing the constraints with CHARMM simulation package (version 37b2)[78]. The peptide sequence has a net positive charge, +7 due to seven LYS and an additional +1 with N-terminal LYS being $NH_3^+$ and C-terminal PHE as $CONH_2$. The peptide coordinates were merged with that of alpha-hemolysin (PDB ID: 7AHL) followed by subsequent rotation and translation to fit it at the trans-end of the pore. As the peptide entry at the trans-end of the pore can be random, the peptide is placed in two vertically opposite orientations depending on the positions of the terminal residues- (State 1) With N- and C-termini pointing towards the cis-end and (State 2) With both termini pointing towards the trans- end of the pore. To accelerate peptide translocation from trans- towards the cis- end within the computational time limit, electric field, $E = 1.034 \times 10^8$ V/m, is applied to the peptide (corresponding to V = +900 mV, an order of magnitude higher than experimental voltage) whereas the pore residues remain subjected to the experimental trans-membrane voltage corresponding to an electric field, $E = 1.034 \times 10^7$ V/m. All the residues of the alpha-hemolysin but the pore lining residues (identified using POREWALKER[79]) are fixed in coordinate space[80]. In addition, unfolding of the CAMAP6 peptide within the geometrical constriction of the pore and subsequent translocation under the effect of electric field was effected using time dependent half quadratic perturbation method (HQBM: Half Quadratic biased Molecular Dynamics module of CHARMM simulation package)[81,82]. A conformational change was forced on the peptide by application of a time-dependent bias on all backbone atoms, moving each of them away from the other, in effect forcing the peptide away from its initial configuration and leading to its unfolding (The force constant of the half harmonic potential, α = 50.0 kcal/molA$^4$). As the protein unfolds completely the protein is translocated up using the same electric field, $E = 1.034 \times 10^8$ V/m. Trajectories for both folded and unfolded peptide range from 40–50 ns depending on the duration for complete translocation. Full atomistic simulation of the translocation process is conducted with CHARMM-27 force field in ACE implicit solvent model (continuum with dielectric constant of 80) using Langevin dynamics (friction coefficient 10 $ps^{-1}$)[83–86] maintaining a constant temperature of 300 K. Van der Waals interactions were computed using switching function with a cutoff of 12 Å. SHAKE algorithm was used to constrain the hydrogen bonds permitting a time step of 2 fs. The formalism for the biased molecular dynamics is being described in details in the SI.


1. Rehling, P. *et al.* Protein insertion into the mitochondrial inner membrane by a twin-pore translocase. *Science* **299**, 1747–1751 (2003).
2. Hessa, T. *et al.* Recognition of transmembrane helices by the endoplasmic reticulum translocon. *Nature* **433**, 377–381 (2005).
3. Hinnah, S. C. *et al.* The chloroplast protein import channel TOC75: pore properties and interaction with transit peptides. *Biophys. J.* **83**, 899–911 (2002).
4. Hetzer, M. W. The Nuclear Envelope. *Cold Spring Harb Perspect. Biol.* **2**, a000539 (2010).
5. Dyer, J. M., McNew, J. A. & Goodman, J. M. The Sorting Sequence of the Peroxisomal Integral Membrane Protein PMP47 Is Contained within a Short Hydrophilic Loop. *J. Cell Biology* **133**, 269–280 (1996).
6. Inamdar, M. M., Gelbart, W. M. & Phillips, R. Dynamics of DNA ejection from bacteriophage. *Biophys. J.* **91**, 411–420 (2006).
7. Majd, S. *et al.* Applications of biological pores in nanomedicine, sensing, and nanoelectronics. *Curr. Opin. Biotechnol.* **21**, 439–76 (2010).
8. Gu, L.-Q. & Shim, J. W. Single molecule sensing by nanopores and nanopore devices. *Analyst* **135**, 441–451 (2010).
9. Kasianowicz, J. J. *et al.* Nanoscopic Porous Sensors. *Annu. Rev. Anal. Chem.* **1**, 737–766 (2008).
10. Wanunu, M. Nanopores: A journey towards DNA sequencing. *Phys. Life Rev.* **9**, 125–158 (2012).
11. DeBlois, R. W. & Bean, C. P. Counting and sizing of submicron particles by the resistive pulse technique. *Rev. Sci. Instrum.* **41**, 909–915 (1970).
12. Oukhaled, A. *et al.* Sensing Proteins Through Nanopores: Fundamental to Applications. *ACS Chem. Biol.* **7**, 1935–1949 (2012).
13. Fologea, D., Ledden, B., McNabb, D. S. & Li, J. Electrical characterization of protein molecules by a solid-state nanopore. *Appl. Phys. Lett.* **91**, 053901 (2007).
14. Movileanu, L. Interrogating single proteins through nanopores: challenges and opportunities. *Trends Biotechnol.* **27**, 333–341 (2009).
15. Li, J. *et al.* Ion-beam sculpting at nanometer length scales. *Nature* **412**, 166–169 (2001).
16. Dekker, C. Solid-state nanopores. *Nat. Nanotechnol.* **2**, 209–215 (2007).
17. Yusko, E. C. *et al.* Controlling Protein Translocation Through Nanopores with Bio-Inspired Fluid Walls. *Nat. Nanotechnol.* **6**, 253–260 (2011).
18. Golovchenko, J. A. *et al.* Graphene as a subnanometre trans-electrode membrane. *Nature* **467**, 190–193 (2010).
19. Movileanu, L., Schmittschmitt, J., Scholtz, J. M. & Bayley, H. Interaction of Peptides with a Protein Nanopore. *Biophys. J.* **89**, 1030–1045 (2005).
20. Asandei, A. *et al.* Investigation of Single-Molecule Kinetics Mediated by Weak Hydrogen-Bonds within a Biological Nanopore. *Langmuir* **27**, 19–24 (2011).
21. Stefureac, R. *et al.* Transport of α-Helical Peptides through α - Hemolysin and Aerolysin Pores. *Biochemistry* **45**, 9172–9179 (2006).
22. Wolfe, A. J. *et al.* Catalyzing the Translocation of Polypeptides through Attractive Interactions. *J. Am. Chem. Soc.* **129**, 14034–14041 (2007).
23. Goodrich, C. P. *et al.* Single-molecule electrophoresis of beta-hairpin peptides by electrical recordings and Langevin dynamics simulations. *J. Phys. Chem. B.* **111**, 3332–3335 (2007).
24. Merstorf, C. *et al.* Wild type, mutant protein unfolding and phase transition detected by single-nanopore recording. *ACS Chem. Biol.* **7**, 652–658 (2012).
25. Mohammad, M. M., Prakash, S., Matouschek, A. & Movileanu, L. Controlling a Single Protein in a Nanopore through Electrostatic Traps. *J. Am. Chem. Soc.* **130**, 4081–4088 (2008).
26. Apetrei, A. *et al.* Unimolecular Study of the Interaction Between the Outer Membrane Protein OmpF from E. coli and an Analogue of the HP (2–20) Antimicrobial Peptide. *J. Bioenerg. Biomembr.* **42**, 173–180 (2010).
27. Lamichhane, U. *et al.* Peptide translocation through the mesoscopic channel: binding kinetics at the single molecule level. *Eur. Biophys. J.* **42**, 363–369 (2013).
28. Pastoriza-Gallego, M. *et al.* Dynamics of Unfolded Protein Transport through an Aerolysin Pore. *J. Am. Chem. Soc.* **133**, 2923–2931 (2011).
29. Oukhaled, G. *et al.* Unfolding of Proteins and Long Transient Conformations Detected by Single Nanopore Recording. *Phys. Rev. Lett.* **98**, 158101 (2007).
30. Manrao, E. A. *et al.* Reading DNA at single-nucleotide resolution with a mutant MspA nanopore and phi29 DNA polymerase. *Nat. Biotechnol.* **30**, 349–353 (2012).
31. Haque, F. *et al.* Real-time sensing and discrimination of single chemicals using the channel of phi29 DNA packaging nanomotor. *ACS Nano* **6**, 3251–3261 (2012).
32. Bezrukov, S. M., Vodyanoy, I. & Parsegian, V. A. Counting polymers moving through a single-ion channel. *Nature* **370**, 279–281 (1994).
33. Kasianowicz, J. J., Brandin, E., Branton, D. & Deamer, D. W. Characterization of individual polynucleotide molecules using a membrane channel. *Proc. Natl. Acad. Sci. USA* **93**, 13770–13773 (1996).
34. Balijepalli, A. *et al.* Theory of Polymer–Nanopore Interactions Refined Using Molecular Dynamics Simulations. *J. Am. Chem. Soc.* **135**, 7064–7072 (2013).
35. Reiner, J. E., Kasianowicz, J. J., Nablo, B. J. & Robertson, J. W. F. Theory for polymer analysis using nanopore-based single-molecule mass spectrometry. *Proc. Natl. Acad. Sci. USA* **107**, 12080–12085 (2010).
36. Robertson, J. W. F. *et al.* Single-molecule mass spectrometry in solution using a solitary nanopore. *Proc. Natl. Acad. Sci. USA* **104**, 8207–8211 (2007).
37. Payet, L. *et al.* Thermal Unfolding of Proteins Probed at the Single Molecule Level Using Nanopores. *Anal. Chem.* **84**, 4071–4076 (2012).
38. Freedman, K. J., Haq, S. R., Edel, J. B., Jemth, P. & Kim, M. J. Single molecule unfolding and stretching of protein domains inside a solid-state nanopore by electric field. *Sci. Rep.* **3**, 1638; DOI:10.1038/srep01638 (2013).
39. Krimizialtin, S., Ganesan, V. & Makarov, D. E. Translocation of a beta-hairpin-forming peptide through a cylindrical tunnel. *J. Chem. Phys.* **121**, 10268–10277 (2004).
40. Huang, L. & Makarov, D. E. Translocation of a knotted polypeptide through a pore. *J. Chem. Phys.* **129**, 121107 (2008).
41. Makarov, D. E. Computer simulations and theory of protein translocation. *Acc. Chem. Res.* **42**, 281–289 (2009).
42. Aksimentiev, A. *et al.* Modeling transport through synthetic nanopores. *IEEE Nanotechnology* **3**, 20–28 (2009).
43. Sathe, C., Zou, X., Leburton, J.-P. & Schulten, K. Computational investigation of DNA detection using graphene nanopores. *ACS Nano* **5**, 8842–8851 (2011).
44. Engelman, D. M. & Steinz, T. A. The spontaneous insertion of proteins into and across membranes: the helical hairpin hypothesis. *Cell* **23**, 411–422 (1981).
45. Keyser, U. F. Controlling molecular transport through nanopores. *J. R. Soc. Interface* **8**, 1369–1378 (2011).
46. Bacci, M., Chinappi, M., Casciola, C. M. & Cecconi, F. Protein translocation in narrow pores: Inferring bottlenecks from native structure topology. *Phys. Rev. E* **88**, 022712 (2013).
47. Bayley, H. *et al.* in *Single Molecules and Nanotechnology* (eds. Rigler, R. & Vogel, H.) Ch. **10**, 251–277 (Springer, 2008).
48. Song, L. Z. *et al.* Structure of staphylococcal alpha-hemolysin, a heptameric transmembrane pore. *Science* **274**, 1859–1866 (1996).

49. Rodriguez-Larrea, D. & Bayley, H. Multistep protein unfolding during nanopore translocation. *Nat. Nanotechnol.* **8**, 288–295 (2013).
50. Bates, M., Burns, M. & Meller, A. Dynamics of DNA molecules in a membrane channel probed by active control techniques. *Biophys. J.* **84**, 2366–2372 (2003).
51. Fologea, D. *et al.* Slowing DNA Translocation in a Solid State Nanopore. *Nano Letters* **5**, 1734–1737 (2005).
52. Meller, A., Nivon, L. & Branton, D. Voltage-driven DNA translocations through a nanopore. *Phys. Rev. Lett.* **86**, 3435–3438 (2001).
53. Anderson, B. N., Muthukumar, M. & Meller, A. pH Tuning of DNA Translocation Time through Organically Functionalized Nanopores. *ACS Nano* **7**, 1408–1414 (2013).
54. Butler, T. Z., Gundlach, J. H. & Troll, M. Ionic current blockades from DNA and RNA molecules in the alpha-hemolysin nanopore. *Biophys. J.* **93**, 3229–3240 (2007).
55. Butler, T. Z., Gundlach, J. H. & Troll, M. A. Determination of RNA orientation during translocation through a biological nanopore. *Biophys. J.* **90**, 190–199 (2006).
56. Wong, C. T. A. & Muthukumar, M. Polymer translocation through α- hemolysin pore with tunable polymer-pore electrostatic interaction. *J. Chem. Phys.* **133**, 045101 (2010).
57. Talaga, D. S. & Li, J. Single-Molecule Protein Unfolding in Solid State Nanopores. *J. Am. Chem. Soc.* **131**, 9287–9297 (2009).
58. Pedone, D., Firnkes, M. & Rant, U. Data Analysis of Translocation Events in Nanopore Experiments. *Anal. Chem.* **81**, 9689–9694 (2009).
59. Di Fiori, N. *et al.* Optoelectronic control of surface charge and translocation dynamics in solid-state nanopores. *Nat. Nanotechnol.* **in press**, doi:10.1038/nnano.2013.221 (2013).
60. Tsutsui, M. *et al.* Trapping and identifying single-nanoparticles using a low-aspect-ratio nanopore. *Appl. Phys. Lett.* **103**, 013108 (2013).
61. He, Y. *et al.* Controlling DNA Translocation through Gate Modulation of Nanopore Wall Surface Charges. *ACS Nano* **5**, 5509–5518 (2011).
62. Wong, C. T. A. & Muthukumara, M. J. Polymer capture by electro-osmotic flow of oppositely charged nanopores. *J. Chem. Phys.* **126**, 164903-1–164903-6 (2007).
63. Yusko, E. C., Billeh, Y. N., Yang, J. & Mayer, M. *in Nanopores: Sensing and Fundamental Biological Interactions* (eds. Iqbal, S. M. & Bashir, R.), Ch. **9**, 203–225, (Springer US 2011).
64. Firnkes, M. *et al.* Electrically facilitated translocations of proteins through silicon nitride nanopores: conjoint and competitive action of diffusion, electrophoresis, and electroosmosis. *Nano Letters* **10**, 2162–2167 (2010).
65. Mereuta, L. *et al.* Protein Nanopore-Based, Single-Molecule Exploration of Copper Binding to an Antimicrobial-Derived, Histidine-Containing Chimera Peptide. *Langmuir* **28**, 17079–17091 (2012).
66. Deaton, K. R., Feyen, E. A., Nkulabi, H. J. & Morris, K. F. Pulsed-field gradient NMR study of sodium dodecyl sulfate micelle–peptide association. *Magn. Reson. Chem.* **39**, 276–282 (2001).
67. Schuck, P., MacPhee, C. E. & Howlett, G. J. Determination of Sedimentation Coefficients for Small Peptides. *Biophys. J.* **74**, 466–474 (1998).
68. Soranno, A. *et al.* Quantifying internal friction in unfolded and intrinsically disordered proteins with single-molecule spectroscopy. *Proc. Natl. Acad. Sci. USA.* **109**, 17800–17806 (2012).
69. Marcinowski, K. J., Shao, H., Clancy, E. L. & Zagorski, M. G. Solution Structure Model of Residues 1–28 of the Amyloid *β*-Peptide When Bound to Micelles. *J. Am. Chem. Soc.* **120**, 11082–11091 (1998).
70. Gu, L.-Q., Cheley, S. & Bayley, H. Prolonged Residence Time of a Noncovalent Molecular Adapter, β-Cyclodextrin, within the β-barrel of Mutant α-Hemolysin Pores. *J. Gen. Physiol.* **118**, 481–493 (2001).
71. Khandogin, J., Chen, J. & Brooks III, C. L. Exploring atomistic details of pH-dependent peptide folding. *Proc. Natl. Acad. Sci. USA* **103**, 18546–18550 (2006).
72. Yang, C. & Li, D. Electrokinetic effects on pressure-driven liquid flows in rectangular microchannels. *J. Colloid Interface Sci.* **194**, 95–107 (1997).
73. Li, T.-D. *et al.* Structured and viscous water in subnanometer gaps. *Phys. Rev. B.* **75**, 115415 (2007).
74. Merrifield, R. B. Chemistry of Amino Acids. *Science* **232**, 341–347 (1976).
75. Lee, D. G. *et al.* Structure−Antiviral Activity Relationships of Cecropin A-Magainin 2 Hybrid Peptide and its Analogues. *J. Peptide Sci.* **10**, 298–303 (2004).
76. Montal, M. & Mueller, P. Formation of bimolecular membranes from lipid monolayers and a study of their electrical properties. *Proc. Natl. Acad. Sci. U S A* **69**, 3561–3566 (1972).
77. Luchian, T., Shin, S.-H. & Bayley, H. Single-molecule covalent chemistry with spatially separated reactants. *Angew. Chem. Int. Ed.* **42**, 3766–3771 (2003).
78. Brooks, B. R. *et al.* The Biomolecular Simulation Program. *J. Comput. Chem.* **30**, 1545–1614 (2009).
79. http://www.ebi.ac.uk/thornton-srv/software/PoreWalker/.
80. Pellegrini-Calace, M., Maiwald, T. & Thornton, J. M. Pore-Walker: a novel tool for the identification and characterization of trans-membrane protein channels from their three-dimensional structure. *PLOS Comp. Biol.* **5**, 1–16 (2009).
81. Paci, E. & Karplus, M. Forced unfolding of fibronectin type 3 modules: An analysis by biased molecular dynamics simulations. *J. Mol. Biol.* **288**, 441–459 (1999).
82. Tian, P. & Bernstein, H. D. Molecular basis for the structural stability of an enclosed β-barrel loop. *J. Mol. Biol.* **402**, 475–489 (2010).
83. Schaefer, M. & Karplus, M. A Comprehensive Analytical Treatment of Continuum Electrostatics. *J. Phys. Chem.* **100**, 1578–1599 (1996).
84. Schaefer, M., Bartels, C. & Karplus, M. Solution conformations and thermodynamics of structured peptides: Molecular dynamics simulation with an implicit solvation model. *J. Mol. Biol.* **284**, 835–847 (1998).
85. Calimet, N., Schaefer, M. & Simonson, T. Protein molecular dynamics with the generalized born/ACE solvent model. *Proteins* **45**, 144–158 (2001).
86. Schaefer, M., Bartels, C., Leclerc, F. & Karplus, M. Effective Atom Volumes for Implicit Solvent Models: Comparison between Voronoi Volumes and Minimum Fluctuation Volumes. *J. Comp. Chem.* **22**, 1857–1879 (2001).


## Acknowledgments

The authors acknowledge the financial support offered by grants PN-II-ID-PCCE-2011-2-0027, PN-II-PT-PCCA-2011-3.1-0595, PN-II-PT-PCCA-2011-3.1-0402, the National Research Foundation of Korea (NRF) grant funded by the Korea government (MEST) (No. 2011-0017532), and the U.S. National Science Foundation (CHE-0548047 and CMMI-0941470).

## Author contributions

L.M. and A.A. carried out the experimental work and analyzed the data, M.R. and I.A. performed the molecular dynamics and simulations tasks, and analyzed the data, J.K.L. and Y.P. synthesized all peptides, T.L. and I.A. supervised the experimental and simulation work, analyzed the data and wrote the main manuscript text. All authors reviewed the manuscript.

## Additional information

**Supplementary information** accompanies this paper at http://www.nature.com/scientificreports

**Competing financial interests:** The authors declare no competing financial interests.

**How to cite this article:** Mereuta, L. *et al.* Slowing down single-molecule trafficking through a protein nanopore reveals intermediates for peptide translocation. *Sci. Rep.* **4**, 3885; DOI:10.1038/srep03885 (2014).